ELSEVIER

Neurobiology of Aging xx (2010) xxx

NEUROBIOLOGY OF AGING

www.elsevier.com/locate/neuaging

Diagnostic power of default mode network resting state fMRI in the detection of Alzheimer's disease

Walter Koch[a,*], Stephan Teipel[b,c], Sophia Mueller[a], Jens Benninghoff[d], Maxmilian Wagner[d], Arun L.W. Bokde[d,e,f,g], Harald Hampel[d,e,f,g], Ute Coates[a], Maximilian Reiser[a], Thomas Meindl[a]

[a] *Institute for Clinical Radiology, University of Munich, Munich, Germany*
[b] *Department of Psychiatry, University of Rostock, Rostock, Germany*
[c] *Deutsches Zentrum für Neurodegenerative Erkrankungen (DZNE), Germany*
[d] *Department of Psychiatry & Alzheimer Memorial Center, University of Munich, Munich, Germany*
[e] *Discipline of Psychiatry, School of Medicine, Trinity College, Dublin, Ireland*
[f] *Trinity College Institute of Neuroscience (TCIN), Laboratory of Neuroimaging & Biomarker Research, Trinity College, Dublin, Ireland*
[g] *The Adelaide and Meath Hospital Incorporating the National Children's Hospital (AMiNCH), Dublin, Ireland*

Received 3 November 2009; received in revised form 7 April 2010; accepted 13 April 2010

Abstract

Functional magnetic resonance imaging (fMRI) of default mode network (DMN) brain activity during resting is recently gaining attention as a potential noninvasive biomarker to diagnose incipient Alzheimer's disease. The aim of this study was to determine which method of data processing provides highest diagnostic power and to define metrics to further optimize the diagnostic value. fMRI was acquired in 21 healthy subjects, 17 subjects with mild cognitive impairment and 15 patients with Alzheimer's disease (AD) and data evaluated both with volumes of interest (VOI)-based signal time course evaluations and independent component analyses (ICA). The first approach determines the amount of DMN region interconnectivity (as expressed with correlation coefficients); the second method determines the magnitude of DMN coactivation. Apolipoprotein E (ApoE) genotyping was available in 41 of the subjects examined. Diagnostic power (expressed as accuracy) of data of a single DMN region in independent component analyses was 64%, that of a single correlation of time courses between 2 DMN regions was 71%, respectively. With multivariate analyses combining both methods of analysis and data from various regions, accuracy could be increased to 97% (sensitivity 100%, specificity 95%). In nondemented subjects, no significant differences in activity within DMN could be detected comparing ApoE ε4 allele carriers and ApoE ε4 allele noncarriers. However, there were some indications that fMRI might yield useful information given a larger sample. Time course correlation analyses seem to outperform independent component analyses in the identification of patients with Alzheimer's disease. However, multivariate analyses combining both methods of analysis by considering the activity of various parts of the DMN as well as the interconnectivity between these regions are required to achieve optimal and clinically acceptable diagnostic power.

Keywords: fMRI; Default mode network; Independent component analysis; Alzheimer's disease

1. Introduction

Imaging neuronal activity using functional magnetic resonance imaging (fMRI) has evolved to an important diagnostic tool to evaluate brain function and neuronal connectivity. A range of studies has described brain regions with synchronous, low frequency blood oxygen level dependent (BOLD) signal changes during rest comprising posterior cingulate/precuneus, medial prefrontal, and bilateral lateral parietal cortex. Because this network is typically deactivated during external stimulation, it has been termed the "default mode network" (default mode network [DMN]) (Binder et al., 1999; Shulman et al., 1997). The behavioral function of this network is still unresolved. It has been suggested that the DMN plays a role in attending to environmental stimuli, as well as mediating processes such as

* Corresponding author at: Institute for Clinical Radiology, University of Munich, Marchioninistr. 15, 81377 Munich, Germany. Tel.: +49 89 7095 3620.
E-mail address: walter.koch@med.uni-muenchen.de (W. Koch).

0197-4580/$ – see front matter © 2010 Elsevier Inc. All rights reserved.
doi:10.1016/j.neurobiolaging.2010.04.013

reviewing past knowledge or preparing future actions. It may also be involved in episodic memory (Greicius et al., 2004).

Interestingly, the DMN regions comprise the typical predilection sites of Alzheimer's disease (AD) (Mosconi, 2005), the most frequent cause of dementia in the elderly, and the most frequent neurodegenerative disorder in humans. Accordingly, resting state fMRI identified significant disruptions in DMN coactivation in patients with AD (Greicius et al., 2004; Rombouts et al., 2009).

Hence, attempts have been made to apply resting state fMRI as a noninvasive, readily available, and radiation exposure-free biomarker of incipient AD (Greicius et al., 2004; Rombouts et al., 2009). Although significant differences were found between patients with AD and healthy controls such as decreased resting-state activity in the posterior cingulate and hippocampus, only few studies described metrics that allow fMRI to be used as a diagnostic procedure on an individual basis (Greicius et al., 2004). It remains unclear, whether clinical acceptable sensitivities and specificities can be achieved and what parameters best discriminate between disease condition and healthy state. This is particularly challenging because there are various data processing methods to extract information about default network activity from fMRI imaging data: correlations of signal time courses between different brain areas using volume of interest (VOI) analyses (Fox et al., 2005; Fransson, 2005) or data-driven extraction of DMN coactivation by independent component analyses (Esposito et al., 2006; Greicius et al., 2004). Most previous studies focused on only 1 way of analysis, leaving the question unanswered, which method achieves highest diagnostic power. Studies comparing both approaches of analysis in healthy controls found different effects of healthy aging on DMN coactivation dependent on the method of processing applied (Bluhm et al., 2008; Greicius et al., 2004). This could potentially interfere with diagnostic power especially in the detection of early stages of disease or preconditions such as mild cognitive impairment (MCI) where subtle changes in network connectivity need to be reliably identified.

In MCI subjects, the presence of a genetic precondition, the apolipoprotein E (ApoE) $\varepsilon 4$ allele has been demonstrated to be a strong predictor in the progression to AD (Buerger et al., 2005; Petersen et al., 1995; Tierney et al., 1996a, 1996b). The ability to detect differences of activity within the DMN between nondemented ApoE $\varepsilon 4$ allele carriers and allele noncarriers could therefore be another sensitive marker for the diagnostic power of each method of analysis.

Aims of this study, therefore, were: (1) to determine the diagnostic power of both methods of analysis of DMN coactivation in resting state fMRI data to distinguish patients with AD from healthy controls; (2) to identify possible alterations in activity within the DMN in ApoE $\varepsilon 4$ allele carriers at risk for development of Alzheimer's disease as well as in subjects with MCI; and (3) to develop optimized metrics by combining information on network alterations in different DMN regions to gain further diagnostic power.

2. Methods

2.1. Subjects

Seventeen subjects with mild cognitive impairment (7 male, 10 female; mean age ± SD, 74.6 ± 7.0 years; age range, 60.4–89.0 years), 15 patients with Alzheimer's disease (8 male, 7 female; mean age ± SD, 76.4 ± 10.3 years; age range, 58.1–100.2 years) and 21 healthy controls (10 male, 11 female; mean age ± SD, 68.6 ± 7.3 years; age range, 56.4–83.0 years) were included in this cross-sectional study. Subjects' consent was obtained according to the Declaration of Helsinki. The study was approved by the ethics committee and the local authorities. All healthy subjects were drug naive concerning medication with possible interference on brain activity, free of neurologic or psychiatric diseases (as assessed by clinical history, psychiatric, neurological, and medical examination, routine blood tests, and a cranial magnetic resonance imaging [MRI] examination, including an anatomical and a fluid attenuation inversion recovery sequence for exclusion of subcortical lesions), without prior head trauma or surgery. Mini Mental State examinations revealed normal results ($\geq$29) in all healthy subjects. All subjects were also tested using the Consortium to Establish a Registry for Alzheimer's disease (CERAD) cognitive battery (Morris et al., 1989). Healthy subjects performed within 1 standard deviation from the age- and education-adjusted mean in all subtests.

AD was diagnosed according to the National Institute of Neurological and Communicative Disorders and Stroke (NINCDS) criteria (McKhann et al., 2001). For the diagnosis of MCI, the Mayo Clinic criteria (Petersen et al., 2001) had to be fulfilled. Only subjects with amnestic MCI were included in this study. AD and MCI patients were free of psychotropic medication.

Solely for the creation of VOI templates for analysis, an additional 12 healthy young volunteers were examined (4 male, 8 female; mean age ± SD, 27.6 ± 2.6 years; age range, 23.3–32.3 years). These had to fulfill the same criteria of normality as stated above for the older healthy controls, except that no CERAD testing was performed.

All subjects (including those for template creation) were right-handed according to the Edinburgh Inventory of Handedness (Oldfield, 1971).

2.2. Apolipoprotein E genotyping

Apolipoprotein E (ApoE) genotyping was performed using a polymerase chain reaction (PCR) kit for the Light Cycler system for real-time PCR (Roche Diagnostics, Mannheim, Germany). Results were available in 17 of the 21 healthy controls, in 15 of the 17 MCI subjects, and in 9 of the 15 AD patients; the other subjects refused genetic

testing. ApoE genotypes observed in healthy controls were ApoE ε2/3 ($n = 2$), ε2/4 ($n = 1$), ε3/3 ($n = 8$), ε3/4 ($n = 5$), and ε4/4 ($n = 1$). ApoE genotypes in MCI subjects were ApoE ε2/2 ($n = 1$), ε3/3 ($n = 9$), ε3/4 ($n = 3$) and ε4/4 ($n = 2$). The genotypes in AD patients, respectively, were determined to be ApoE ε2/3 ($n = 1$), ε3/3 ($n = 4$), ε3/4 ($n = 4$). For further analyses of the genotype effect, subjects were categorized into ApoE ε4 carriers and ApoE ε4 non-carriers.

2.3. fMRI imaging

To determine the coactivation of the default resting state network, all participants underwent fMRI imaging. A resting-state echo-planar gradient-echo functional imaging sequence (rsEPI), followed by a high-resolution anatomical sequence was acquired.

All imaging was acquired on a clinically-approved 3.0 Tesla TRIO MRI scanner (Siemens, Erlangen, Germany) with a maximum gradient strength of 45 millitesla per meter and a maximum slew rate of 200 T/m/s equipped with a 12-element head coil. Functional imaging was obtained with a BOLD-sensitive echo-planar gradient-echo (EPI) sequence using the following imaging parameters: repetition time (TR) 3000 ms, echo time (TE) 30 ms, flip angle (FA) 90°, spatial resolution $3 \times 3 \times 4$ mm^3, imaging matrix 64×64, field-of-view (FoV) 192×192 mm^2, number of slices 28, 120 volumes, acquisition time (TA) 6 minutes. Functional images were scanned in axial orientation and covered the whole brain. For anatomical reference, a high-resolution magnetization-prepared gradient-echo (MPRAGE) sequence was additionally acquired with the following specifications: field of view 256×240 mm^2, spatial resolution $1 \times 1 \times 1$ mm^3, repetition time 14 ms, echo time 7.61 ms, flip angle 20°, number of slices 160, acquisition time 4:50 minutes. Before functional imaging started, the field was shimmed using automated algorithms of the scanner. Subjects were instructed to keep their eyes closed and not to think of anything particular during the functional scans.

2.4. Data preprocessing

Imaging data were initially stored on the institution's picture archiving and communicating system, and were subsequently transferred to a stand-alone evaluation platform (WindowsXP, Microsoft, Redmond, Washington). Image postprocessing and voxel-wise statistical analyses were performed using BrainVoyagerQX® 1.9 (BrainInnovations BV, Maastricht, The Netherlands). The first 5 functional volumes of each time series were discarded to account for T1 saturation effects. Preprocessing included slice-scan time correction using "sinc" interpolation. Data were motion corrected (BrainVoyagerQX® 3-D algorithm) to minimize effects of head motion on analyses. To improve signal detection, temporal and spatial filtering was applied. Drift removal was done using a high-pass temporal filter (3 cycles/run, equivalent to 0.008 Hz). High-frequency fluctuations were removed with a 4-second full-width at half maximum Gaussian kernel. Functional data were coregistered to the individual high-resolution magnetization-prepared gradient-echo (MPRAGE) sequence. In an initial alignment step, the functional and anatomical datasets were coregistered based on the spatial position information recorded by the magnetic resonance scanner. Afterward, fine adjustment was made applying the BrainVoyagerQX® intensity-driven multiscale alignment procedure. The results of the alignment process were inspected visually and corrected manually where necessary. Talairach transformation (Talairach, 1988) of the anatomical dataset was done manually by aligning the sagittal dataset with stereotactic axes (anterior and posterior commissure) and defining the extreme points of the cerebrum. The resulting Talairach transformation matrix was applied both to anatomical and functional images (with resampling of voxels to $1 \times 1 \times 1$ mm^3). Spatial smoothing was achieved by applying a 4 mm full-width at half maximum Gaussian filter.

Information on resting state activity within the DMN was then extracted using 2 different approaches, 1 being purely data driven using independent component analysis to extract functional patterns of synchronized neural activity, the other using volumes of interest to correlate signal changes over time in specific areas as direct measure of functional connectivity. The first approach is capable of detecting any patterns of synchronous activity (including, but not limited to activity within the DMN) without prior hypotheses, whereas the second method enables measurements of connectivity strength between previously identified cortical regions.

2.5. Data-driven analysis approach (independent component analysis)

Single-subject independent component analysis (ICA) was applied to the preprocessed functional datasets using the "FastICA" fixed-point algorithm developed by Hyvarinen et al., implemented as a C^{2+} plug-in for BrainVoyagerQX® (Esposito et al., 2005; Goebel et al., 2006). Before ICA decomposition, the initial dimension of each time series (115 time points/experiment) was preliminarily reduced to 30 by principal component analyses. Afterward, 30 components were extracted by ICA for each subject. From this set, the DMN component was identified observer-independently using self-organizing clustering (Esposito et al., 2005). Briefly, this approach combines datasets from multiple subjects into a single aggregate dataset based upon a measure of similarity between components. The resulting clusters were then visually analyzed for typical DMN coactivation patterns (applying the same criteria as for the manual verification described further below) and the DMN component of each subject determined. The determined DMN components of each subject were then reviewed independently by 2 readers to confirm the presence of typical resting-state net-

work patterns, defined as coactivation of the posterior cingulate cortex, the anterior cingulate cortex, and bilaterally the inferior parietal lobule. These regions were selected as they not only comprise the largest regions of activity within the DMN but also can be identified easily in healthy subjects. Data were also analyzed visually for potential decomposition of the DMN coactivation into more than 1 ICA component, a phenomenon reported previously (Damoiseaux et al., 2006, 2008; Rombouts et al., 2009).

The strength of coactivation was then quantified by measuring BOLD signal intensities in the DMN component map using volumes of interest (VOIs) for each area comprising the DMN. For this purpose we adopted the VOI map validated in a previous study for DMN analysis in young and older healthy controls (Koch et al., 2010). Being based on independent healthy volunteers, the standardized VOI map allows standardized analyses of the patient population presented here. In brief, these VOIs were delineated based on extracted DMN components of the 12 young healthy volunteers by applying a threshold for z values of $\pm$ 0.5. Details can be found in (Koch et al., 2010), the volumes of interest as well as their size and spatial positions are summarized in Table 1. We confirmed previously, that although created in young subjects, this VOI map also fully covers DMN areas of healthy adults. To determine the DMN coactivation from the ICA component, the z values of all voxels in the corresponding volume of interest were averaged.

2.6. Signal time course correlation approach

The average signal time course of each region of the DMN was extracted by applying the identical VOI map to each subject's functional preprocessed scan across the full length of the scan. To reduce potential effects of patient movement during the scan or signal fluctuation resulting other than from activity within the DMN, this step was performed on movement corrected, spatially and temporally filtered imaging data. The extracted signal time courses of each subject were then cross-correlated region by region, Pearson's correlation coefficients were calculated and square correlation matrices were generated (10×10) from these values for each subject. For each group (healthy subjects, subjects with MCI, and patients with AD), these correlation coefficients were then combined across subjects by using the Hedges and Olkin fixed effect model for meta-analyses of r values (Hedges and Vevea, 1998). Based on both groups' meta-analysis correlation matrices, gray scale coded correlation matrices graphs (indicating the strength of interconnectivity between different regions of the DMN) as well as a graph visualizing the group differences were generated for visualization.

Table 1
Talairach coordinates (center of gravity) and sizes of the 3-dimensional volumes of interest used for both quantification of independent component analyses (ICA) components and time course correlation analyses

Default mode network region	Talairach coordinates			Size (voxels)
	X	Y	Z	
Anterior cingulate cortex (ACC)	0	45	17	22,484
Posterior cingulate cortex (PCC)	−2	−53	22	28,368
Left lateral parietal cortex (LPC_L)	−43	−66	20	4302
Right lateral parietal cortex (LPC_R)	45	−61	17	4330
Left superior frontal gyrus (SFG_L)	−20	19	52	1207
Right superior frontal gyrus (SFG_R)	25	17	51	1534
Left medial temporal cortex (MTC_L)	−57	−11	−9	1740
Right medial temporal cortex (MTC_R)	53	−7	−11	2257
Left hippocampus ($HIPP_L$)	−21	−16	−14	634
Right hippocampus ($HIPP_R$)	21	−19	−12	302

2.7. Group comparison

For visual analysis, group-level ICA maps were generated by averaging the DMN components of all subjects of each group. In addition voxel-wise t test statistics were calculated with correction for multiple comparisons following the Benjamini and Hochberg false discovery rate approach (Benjamini and Hochberg, 1995).

To compare quantitative BOLD signal intensities (derived from the data-driven approach) we performed 2-tailed t test ($p \leq 0.05$) between the healthy subjects and subjects with MCI and between healthy controls and patients with AD, respectively. Normality of data was confirmed by calculating skewness and kurtosis as well as Kolmogorov-Smirnov tests. Similarly, for the signal time course analyses, 2-sample 2-tailed t tests (assuming unequal variance; $p \leq 0.05$) were calculated for all potential connections represented in the correlation matrices between both groups. Fischer z transformation was applied to the correlation coefficients to obtain normal distributed data for the random effects analysis. To account for multiple comparisons, the false discovery rate was controlled for in all presented analyses using the Benjamini and Hochberg method (Benjamini and Hochberg, 1995).

To test whether fMRI could possibly identify alterations of activity within the DMN in patients at risk for the development of Alzheimer's disease, DMN coactivation and DMN interconnectivity was compared between ApoE ε4 carriers and noncarriers in a combined analysis including healthy controls and subjects with MCI (but with exclusion of AD patients) using t tests.

2.8. Diagnostic power of the different methods of analyses

To evaluate the diagnostic power of both methods to detect AD, discriminant analyses were run on healthy controls and patients with AD including: (1) only z-transformed correlation coefficients from the signal time course correlation analyses; and (2) only DMN coactivation from ICA analyses. To combine the diagnostic power of both approaches, a third analysis was performed allowing quantitative results of both evaluation methods to be included.

Discriminant analyses are able to determine the linear combination of parameters which best separates both groups of subjects and to estimate the probability a subject belongs to either the patients group or the healthy controls based on the parameters entered. Parameters used for the discrimination were automatically entered using the Wilks λ stepwise variable selection method. We believe that by allowing the inclusion of multiple parameters, results are more meaningful than simple receiver operating characteristic analyses based on measurements obtained by a single area of the DMN.

Diagnostic power is given as sensitivity, specificity, positive predictive value (PPV), negative predictive value (NPV), and accuracy obtained using the discriminant analysis group classification. To give a better estimate of what diagnostic power would be in new subjects to be scanned (for example in a potential routine diagnostic setting), the results presented are those obtained after leave-1-out cross-validation.

In addition, and as for reference, the best diagnostic power achieved with information of a single DMN region (for the ICA method) or a single interregional correlation coefficient (for the time course correlation analyses) to differentiate both groups was determined. For this purpose, the parameter with highest area under the curve (AUC) in receiver operating characteristics (ROC) was selected and sensitivities as well as specificities determined by entering this single factor in a discriminant analysis similarly as in the multivariate models described above.

Because MCI subjects are a heterogeneous group (some ApoE ε4 allele carriers, no follow-up to identify potential conversion to AD), predictive models were only created based upon the data of AD patients and healthy controls. However, to evaluate, to which extent this technique could also detect typical AD patterns in subjects with MCI, the model with highest diagnostic power was also applied to MCI subjects.

No direct comparison analyses between the MCI and the AD group were performed, as the resulting discriminant analysis models would only be optimized to differentiate between those 2 patient groups and not trained to further differentiate patients from healthy subjects. Furthermore, the differentiation between MCI versus AD is mainly based on clinical findings such as the relevance of the impairment for the patient's daily living.

3. Results

All subjects tolerated scanning well. No datasets needed to be discarded due to artifacts. Subjects with MCI or AD were on average 6–7 years older than healthy subjects; this difference is statistically significant ($p = 0.015$, 1-way analysis of variance and defined posthoc contrasts). Posthoc contrasts did not reveal significant age differences between subjects with MCI and AD patients. Even if we did not consider the observed age difference clinically relevant, we allowed the stepwise inclusion algorithm of the discriminant analyses to also select age as a cofactor in the model generation. However, age showed no relevant contribution to any of the models and was rejected by the Wilks λ selection algorithm.

3.1. Data-driven analyses (visual, voxel-wise and quantitative evaluations)

Self-organizing clustering could successfully determine the DMN component in all subjects, as confirmed by visual analyses. The review of the 30 components of each subject did not reveal decomposition of the default network coactivation into more than 1 component.

The results of the quantitative evaluation of DMN coactivation for all 3 groups are given in Table 2 and Fig. 1.

In the healthy subjects, group-level ICA revealed the known default-mode network pattern with coactivation of the anterior and posterior cingulate cortex and connections to the parietal lobule and the frontal lobe bilaterally.

In the MCI group, spatial extent of the coactivated areas of the anterior cingulate cortex (ACC) and the parietal lobule was lower compared with healthy elderly subjects. In AD patients, coactivations of most DMN regions were lower than in healthy controls (Figs. 1 and 2).

3.1.1. Observed quantitative changes in subjects with MCI

In comparison with healthy controls, in subjects with MCI measured DMN activations were slightly lower in

Table 2
Default mode network (DMN) coactivation in healthy controls, patients with mild cognitive impairment (MCI), and patients with Alzheimer's disease (AD) as determined by independent component analyses

DMN	Healthy controls		MCI			AD		
Region	Mean	SD	Mean	SD	*p*	Mean	SD	*p*
ACC	.87	.50	.66	.39	.157	.49	.59	.046
PCC	1.03	.64	1.07	.54	.837	.89	.63	.525
LPC_L	1.12	1.03	1.21	1.08	.791	1.10	1.13	.954
LPC_R	.78	.92	.77	.82	.988	.49	.89	.356
SFG_L	.74	.74	.58	.49	.466	.74	.64	.990
SFG_R	.44	.55	.47	.69	.880	.29	.63	.455
MTC_L	.45	.56	.16	.43	.085	.10	.38	.047
MTC_R	.35	.34	.09	.35	.026	.15	.46	.150
$HIPP_L$	.65	.63	.24	.43	.030	.37	.55	.183
$HIPP_R$	.22	.46	.12	.39	.489	.11	.56	.546

Potential differences of patients with MCI and AD in comparison with healthy controls were tested for significance with 2-tailed *t* tests. *p*-values given are without correction for multiple testing. Controlling for the false discovery rate, none of the results remained significant.
Key: ACC, anterior cingulate cortex; $HIPP_L$, left hippocampus; $HIPP_R$, right hippocampus; LPC_L, left lateral parietal cortex; LPC_R, right lateral parietal cortex; MTC_L, left medial temporal cortex; MTC_R, right medial temporal cortex; PCC, posterior cingulate cortex; SFG_L, left superior frontal gyrus; SFG_R, right superior frontal gyrus.

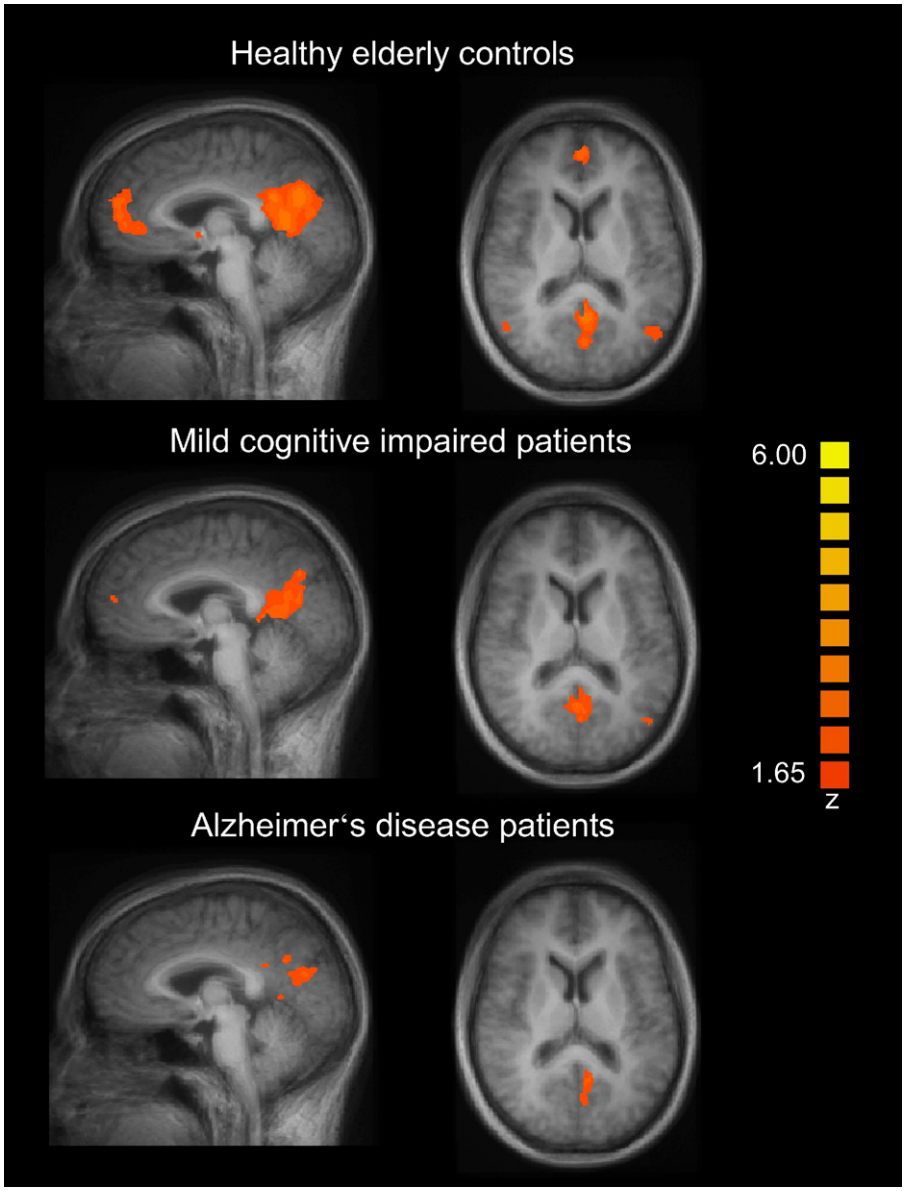

Fig. 1. Magnitude of default mode network (DMN) co-activation in patients with Alzheimer's disease (AD), patients with mild cognitive impairment (MCI) and healthy controls (slices located at Talairach coordinates x = −3, z = 12). Group comparisons are depicted in Fig. 2.

some regions, such as in the medial temporal cortex of both hemispheres. However, none of the differences reached statistical significance.

3.1.2. Observed quantitative changes in patients with AD

Patients with AD showed lower activity within the DMN than healthy controls in all evaluated regions (except for the left superior frontal gyrus) with differences particularly being observed in areas predominantly affected by the disease such as parietal and temporal cortex. However, owing to high standard deviations (both in patients and in healthy controls), none of the differences reached the level of significance.

3.1.3. Influence of ApoE risk allele on activity within the DMN

In nondemented subjects, no significant differences in DMN coactivation could be detected comparing ApoE ε4 allele carriers and ApoE ε4 allele noncarriers (Table 3). Additional discriminant analyses were not able to identify variables with enough power to distinguish allele carriers from allele noncarriers.

3.2. Signal time course analyses results

Based upon correlations of signal time courses, the strength of connectivity between different areas of the DMN is shown in Fig. 3 for healthy controls, subjects

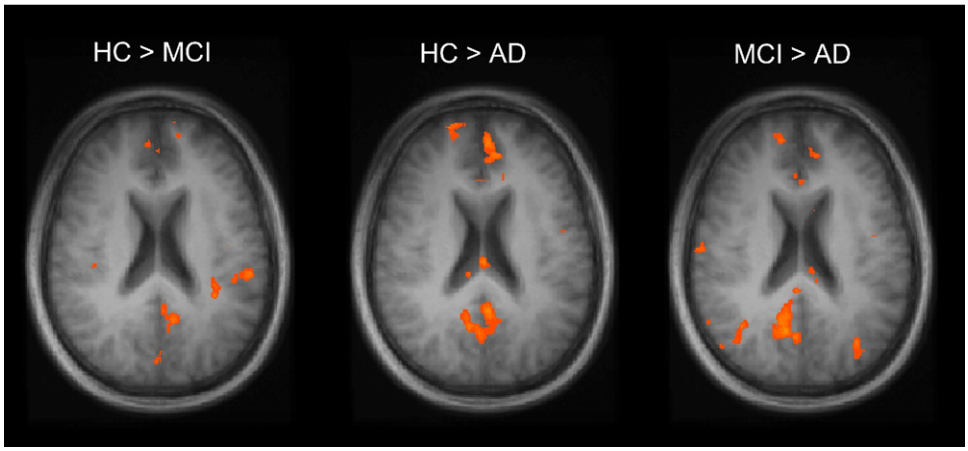

Fig. 2. Group comparisons of default mode network (DMN) co-activation between healthy controls (HC), patients with Alzheimer's disease (AD) and patients with mild cognitive impairment (MCI) based on voxel-wise *t* tests ($p < 0.05$, slices level at Talarach z = 21). Inverse contrasts (MCI < HC, AD < HC and AD < MCI) did not reveal significant differences between groups.

with MCI and with AD. In healthy controls a typical pattern of DMN interconnectivity showing high to moderate interconnectivity of all areas of the DMN could be observed. Even interhemispheric connectivity was high for most components of the network. Highest correlation coefficients were found for the correlations of the posterior cingulate cortex (PCC) with the lateral parietal lobes; lowest correlation coefficients were found for interconnections of the hippocampus with any other DMN region.

3.2.1. Observed changes in subjects with MCI

No clear differences of DMN interconnectivity could be identified between subjects with MCI and healthy controls. For some regions, a tendency to lower connectivity in patients compared with healthy controls could be observed: left hippocampus with PCC (uncorrected $p = 0.028$), right superior frontal cortex with PCC (uncorrected $p = 0.044$), right lateral parietal cortex with right superior frontal cortex (uncorrected $p = 0.044$), and left medial temporal cortex with ACC (uncorrected $p = 0.036$). These differences did not reach the level of significance when correcting for multiple comparisons.

Table 3
Magnitude of default mode network (DMN) coactivation in ApoE ε4 allele carriers and ApoE ε4 allele noncarriers as determined by independent component analyses

DMN	ε4 allele carriers		ε4 allele noncarriers		*t* test
Region	Mean	SD	Mean	SD	*p*
ACC	.88	.43	.56	.48	.065
PCC	1.03	.59	1.01	.60	.943
LPC_L	.98	.87	1.27	1.08	.417
LPC_R	.64	.76	.96	1.06	.337
SFG_L	.65	.59	.60	.67	.813
SFG_R	.44	.65	.50	.60	.807
MTC_L	.46	.54	.22	.54	.239
MTC_R	.21	.33	.31	.47	.519
$HIPP_L$	.52	.47	.30	.78	.331
$HIPP_R$	.16	.48	.02	.20	.354

Potential differences were tested for significance with 2-tailed *t* tests. None of the results were significant.
Key: ACC, anterior cingulate cortex; $HIPP_L$, left hippocampus; $HIPP_R$, right hippocampus; LPC_L, left lateral parietal cortex; LPC_R, right lateral parietal cortex; MTC_L, left medial temporal cortex; MTC_R, right medial temporal cortex; PCC, posterior cingulate cortex; SFG_L, left superior frontal gyrus; SFG_R, right superior frontal gyrus.

3.2.2. Observed changes in patients with AD

Interconnectivity of almost all DMN regions was lower in AD patients than in healthy controls (the only exception being the association between right medial temporal gyrus and right hippocampus) with many of these differences reaching the level of significance (Fig. 3).

Differences were most accentuated in connections originating from the parietal cortex and the superior frontal cortex.

3.2.3. Influence of ApoE risk allele on DMN connectivity

t tests revealed no significant differences in connectivity between both groups of nondemented subjects. Additional discriminant analyses with stepwise inclusion of variables were not able to identify variables with enough power to distinguish allele carriers from allele noncarriers.

3.3. Diagnostic power of both methods of analyses

In ICA, the best single parameter to differentiate between healthy controls and patients with AD was activity within the DMN in the anterior cingulate cortex. The AUC of a receiver operating characteristics analysis for this parameter was 0.702 (95% confidence interval, 0.523–0.880) resulting in poor sensitivity (53.3%) and specificity (71.4%). The multivariate approach using discriminant analyses was unable to identify additional regions to further increase sensitivity or specificity (Table 4).

For the time course correlation analyses, connectivity of the PCC with the superior frontal cortex showed highest

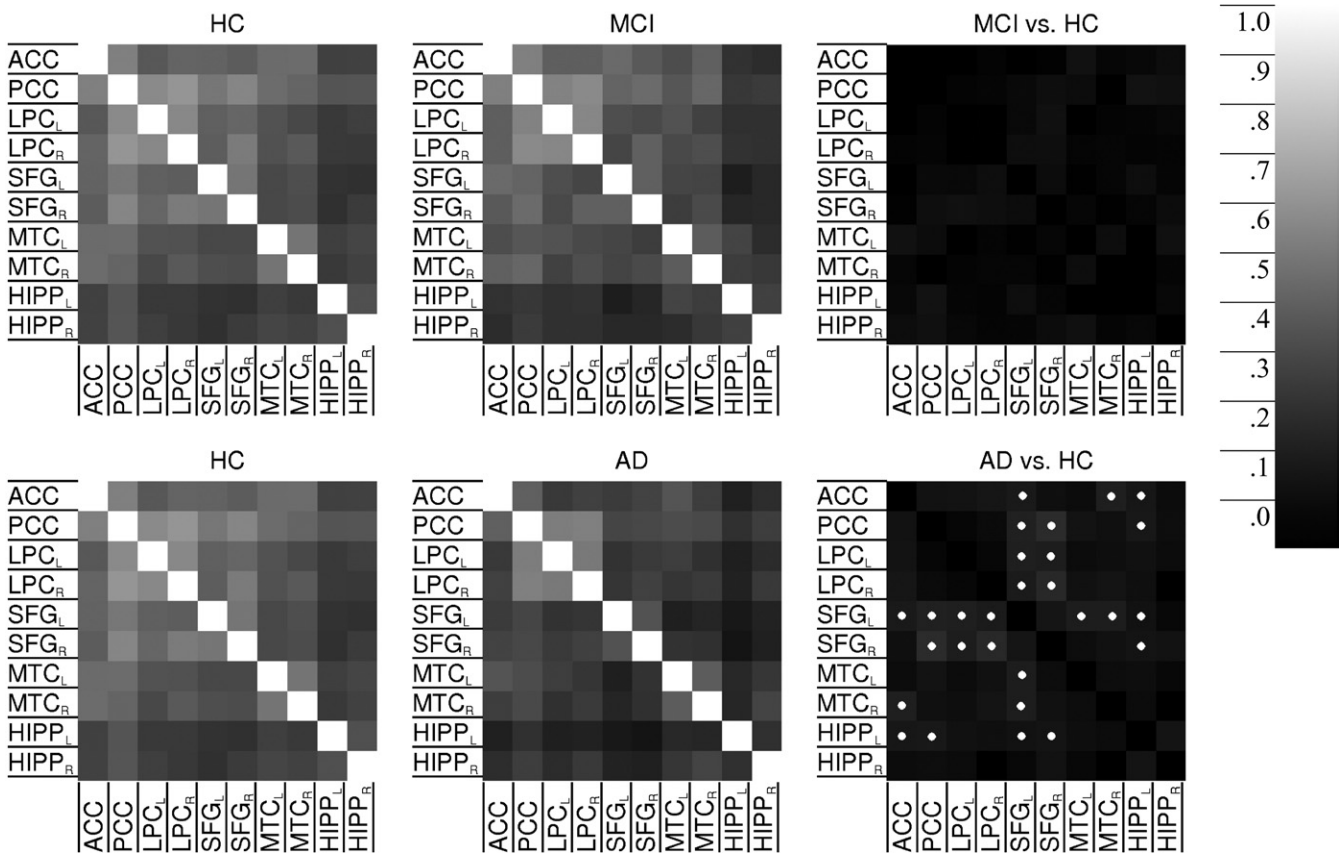

Fig. 3. Correlation matrices representing default network functional connectivity in healthy controls (HC), patients with mild cognitive impairment (MCI), and with Alzheimer's disease (AD). Darker boxes represent low Pearson correlation coefficients between regions, whereas lighter boxes represent stronger correlations. The comparison (last column) shows the respective group differences. Statistical significant group differences are marked with white dots, in all of them connectivity being higher in HC than in AD subjects. For abbreviations please refer to Table 1.

diagnostic power. The respective AUC was 0.848 (95% confidence interval, 0.719–0.976), resulting in a sensitivity of 73.3% and a specificity of 71.4%. Discriminant analyses were able to predict the correct diagnoses from multiple time course correlation parameters, leading to a reasonable gain in sensitivity and specificity (Table 4). The resulting model is comprised of the following interconnections between DMN regions: right medial temporal cortex (MTC_R) with left medial temporal cortex (MTC_L), right medial temporal cortex with right hippocampus ($HIPP_R$), right superior frontal gyrus (SFG_R) with PCC, right superior frontal gyrus with left medial temporal cortex, and left hippocampus ($HIPP_L$) with PCC.

By combining results of both methods of analyses (ICA and time course analyses), diagnostic power could further be increased (Table 4). This "combined" model includes the identical connections as described above for the time course analyses but with the addition of ACC and PCC activity derived from ICA, achieving a sensitivity of 100% with a specificity of 95% (Table 4). All given values are cross-validated, indicating high validity of all described generated models.

Next, the "combined" model was applied to MCI subjects without further modification or optimization, to verify whether the characteristics of AD patients could also be detected in MCI subjects. This procedure classified 11 of the

Table 4
Diagnostic power of signal time course analyses and independent component analyses in the differentiation of healthy controls from patients with Alzheimer's disease

Method	Sensitivity	Specificity	PPV	NPV	Accuracy
Time course correlation analyses	86.7%	95.2%	92.9%	90.9%	91.7%
Independent component analyses	53.3%	71.4%	57.1%	68.2%	63.9%
Combination of both approaches	100.0%	95.2%	93.8%	100.0%	97.2%

All values are derived from discriminant analyses with stepwise parameter inclusion and leave-1-out cross-validation.
Key: NPV, negative predictive value; PPV, positive predictive value.

17 MCI subjects as pathologic, resulting in a sensitivity of 64.7%, a specificity of 95.2%, positive and negative predictive values of 91.7% and 76.9%, as well as an accuracy of 81.6%.

4. Discussion

Although fMRI of the DMN under resting conditions has been examined as a marker to differentiate patients with AD from healthy elderly controls (Greicius et al., 2004; Rombouts et al., 2009), little is known about the diagnostic power of the available methods of analyses. The interconnectivity of different parts of the DMN can be evaluated using VOI based time course analyses. Alternatively, the network can be extracted en bloc to determine the magnitude of coactivation of the network components.

To our knowledge, our study is the first to directly compare these methods of analysis to determine their diagnostic power in the detection of subjects with MCI or AD and to define optimized models to differentiate patients from healthy controls on an individual basis. The methods used to analyze the data were specifically designed for this purpose, observer-independent, and are readily available also on other imaging equipment.

4.1. Differentiating patients with AD from healthy controls

In terms of diagnostic power to identify patients with Alzheimer's disease, the use of simple time course analyses was superior to ICA. ICA demonstrated lower activity within the DMN in AD patients in most regions (particularly in the parietal and temporal lobes, as well as in the hippocampus regions), but none of the differences observed reached the level of significance. The pattern of the trends observed, however, resembles the pattern typically observed in patients with AD in positron emission tomography (PET) studies (Minoshima et al., 1997; Mosconi et al., 2007, 2008; Mosconi, 2005) and in other fMRI studies (Greicius et al., 2004; Rombouts et al., 2009; Sorg et al., 2007) where a typical pattern of progress, starting with pathology in the temporomesial cortex with further spread through the cingulate cortex, parietal lobes, and later on, the frontal lobes was described. Furthermore, the regions with diminished activity within the DMN are the same as those identified with high amyloid load in AD patients by neuropathology and neuroimaging studies (Braak and Braak, 1991; Buckner et al., 2005; Nordberg, 2004, 2008). Despite these factors, simple VOI measurements of activity within the DMN in ICA maps performed poorly as a diagnostic tool (sensitivity 53.3%, specificity 71.4% for activity within the DMN in the anterior cingulate), owing to the high variability of values in different subjects. The latter may most probably be attributed to the variability of perfusion and metabolism, as previously described in PET studies (Phelps et al., 1983), or to partial volume effects due to brain volume loss in patients (due to neurodegeneration) in comparison with healthy controls (Whitwell and Jack, 2005).

If, on the other hand, DMN interconnectivity based on signal time course correlations is considered, connectivity between most DMN regions was significantly lower in patients with AD than in controls. Again, these effects were mainly observed for connections of the anterior and posterior cingulate cortex, with the superior frontal gyrus and with the parietal lobe, matching the expected disease pattern. Our results are in line with the results presented by Wang et al. (2007), who also described various significantly disturbed connections in AD patients. However, the total amount of connections reaching the level of significance was lower in our data due to fewer regions analyzed in our study (more DMN selective placement of VOIs) and the correction for multiple testing applied. The best single parameter to differentiate between AD and healthy controls was the connection of the posterior cingulate cortex with the superior frontal cortex. This supports a hypothesis of anterior-posterior disconnection in AD as described in PET studies (Grady et al., 2001; Horwitz et al., 1987). Still, the diagnostic power (sensitivity of 73.3% and a specificity of 71.4%) using this parameter is only moderate, and may not meet the level of acceptance in a clinical setting.

Single DMN regions or interconnectivity between DMN regions therefore appear to be of limited diagnostic value. However, the DMN consist of a considerable amount of different regions and interregional connections (Fox et al., 2005; Fransson, 2005; Wang et al., 2007). We therefore hypothesized, that a multivariate approach considering information from several of the DMN regions could further increase diagnostic power. We tested this with discriminant analyses, allowing variables with potential to discriminate patients from healthy controls to be automatically selected and a model with best discriminative capacity to be generated. Such an approach is only feasible with quantitative or semiquantitative data and cannot be readily transferred to visual analyses. On the other hand, it guarantees high observer-independency, a substantial prerequisite for routine clinical use.

The multivariate analyses used various DMN regions to predict the correct diagnosis, including some interhemispheric connections. Again, connections with regions typically involved by the AD pathology contributed most to the differentiation between disease and healthy state. This approach, based on VOI data and a mathematical model, differs considerably from that chosen by Greicius et al. (2004) who introduced a goodness-of-fit metric to compare the similarity of an individual DMN ICA map with a normal reference template. With this metric, Greicius et al. achieved a considerably high diagnostic power (sensitivity 85% and specificity 77%). The approach also allowed consideration of all DMN regions for the differentiation of AD and healthy controls (HC), but it is neither able to exclude regions with low informative value for the differentiation

nor weight the contributions of each factor to optimize performance. In addition, the discriminant analyses introduced in our study allows us to combine different types of information in a single equation, including any combination of parameters obtained from ICA maps and that of time course correlation analysis.

These considerations are of particular importance, as ICA and time course analyses may provide different information on the DMN, which, in combination, may further increase diagnostic power. ICA extracts the network en bloc, resulting in a measure correlating with DMN coactivation magnitude (McKeown et al., 1998), signal time course analyses, on the other hand, reflect the amount of connectivity between different parts of the DMN (Fox et al., 2005), but may be less specific for the DMN. The combination of both approaches (the "combined" model) was able to achieve an excellent diagnostic power with a sensitivity of 100.0% and a specificity of 95.2%.

4.2. Differentiating subjects with MCI from healthy controls

In MCI subjects, neither ICA nor time course analyses could identify DMN alterations compared with healthy controls. However, some trends could be observed, particularly a tendency to a disruption in the connection between the left hippocampus and the PCC, which only missed the level of significance due to correction for multiple testing. Similar (but significant) findings were described by Sorg et al. (2007) and Wang et al. (2006). This reduced connectivity between the hippocampus and the PCC constitutes the basis of the "disconnection hypothesis" (Delbeuck et al., 2003), and is considered responsible for decreased metabolism in the PCC in early AD (Minoshima et al., 1997) typically observed in PET studies.

Applying the multivariate "combined" model developed for the identification of patients with AD to the data of MCI subjects, the approach identified an AD typical pattern in 11 of 17 subjects. This well resembles the percentage of MCI subjects presenting with an AD typical pattern (79% of subjects with deficits in multiple cognitive domains and 31% of patients with amnesic MCI) in a recent large multicenter PET study (Mosconi et al., 2008). Because the model used in our study is only optimized for the detection of patients with AD, the observed sensitivity (65%) and specificity (95%) of this approach is of limited predictive value for the application in new patients. Furthermore, the heterogeneous nature of subjects with MCI needs to be kept in mind, limiting also the power of neurophysiological tests (Knopman et al., 2001). MCI can be a precondition of AD with a probability of conversion to AD of 10%–15% per year (Artero et al., 2003; Petersen, 2004), but it can also be caused by vascular disease or even observed in healthy aging (Petersen et al., 2001, 2004). Much effort has been put forward to both understand the underlying pathology in this risk group and to differentiate between later converters and nonconverters. Fluorodesoxy glucose PET has already proven to be a valuable tool for this differentiation (Drzezga et al., 2003, 2005; Minoshima et al., 1997). The strong association between metabolism and neuronal activity (Phelps et al., 1983) also suggests a potential predictive power of fMRI. As currently no follow-up is available for our MCI subjects, we cannot comment on whether subjects identified with AD pattern in our multivariate analysis have a higher chance of conversion to AD than those without AD pattern. Nevertheless, the proportion of ApoE ε4 allele carriers (a potential risk factor for the development of AD) was higher in MCI subjects with AD pattern (4 of 7) than in those without (1 of 3) supporting the applicability of this approach to identify subjects with highest risk of conversion. On the other hand, the pure presence of the ApoE ε4 allele did not result in measurable effects on the DMN in resting state fMRI. Further prospective studies with follow-up will be needed to clarify this issue.

In a previous project, we compared ICA and time course analyses in healthy young and healthy older subjects and found a higher sensitivity of ICA to detect effects of physiologic aging (Koch et al., 2010) on activity within the DMN. We hypothesized, that this could either be interpreted as higher sensitivity of ICA to detect subtle changes of activity within the DMN, or, contrary could indicate higher tolerance of time course analyses to effects of healthy aging. Our current results now indicate a higher diagnostic power of time course analyses in the detection of AD. This, in conjunction with our previous results, favors the second hypothesis: time course analyses seem to be less affected by age effects than ICA, while still conserving their ability to detect neurodegenerative loss of network integrity. Diagnostic power of ICA might suffer more than time course analyses from variability introduced by BOLD signal loss with aging such as related to decline of both cerebral metabolism and perfusion with aging (De Santi et al., 1995; Horwitz et al., 1987; Willis et al., 2002) or partial volume effects due to gray matter loss with aging (Conde and Streit, 2006; Good et al., 2001; Raz et al., 1997). These considerations also led us to define the VOI map for analyses based on independent young subjects, to reliably cover the full extent of each DMN region.

4.3. Limitations

Some limitations have to be considered when interpreting the data presented. First, our data applies only to resting state default network coactivation, hence we cannot comment on the diagnostic power of task-dependent DMN deactivations. Resting state is much easier and more reliable to accomplish in a potential routine setting with patients. Issues such as performance differences among patients and practice effects with repeated scanning are minimized acquiring only resting state functional imaging.

Second, although subjects were instructed to lie calm during scanning and not to think of anything particular, the

compliance with these resting state conditions could not be monitored and specific brain activity interference could not entirely be excluded.

Third, cardiac and respiratory pulsations may generate BOLD signal variation that projects into areas resembling the DMN (Birn et al., 2006). The ICA can to some extent separate the distinct temporal pattern generated by these factors from the signal changes due to activity within the DMN (Beckmann and Smith, 2005; De Luca et al., 2006; Fukunaga et al., 2006). However, even with the temporal filtering applied to our data before remaining analysis, influences on the correlation analyses cannot be entirely excluded.

Fourth, from the stack of 30 components extracted by the data-driven ICA approach, only 1 component was selected for further analysis, following the concept of several other publications (Esposito et al., 2006; Garrity et al., 2007; Greicius et al., 2007). A potential decomposition of DMN coactivation into more than 1 component (as observed in some studies [Damoiseaux et al., 2006, 2008; Rombouts et al., 2009]) cannot be accounted for in this concept, however, visual inspection did not reveal this phenomenon in our data.

Fifth, the number of subjects in this study is limited and complex models were used to generate a procedure with optimized diagnostic power. Even though cross-validation confirms a high validity of the method described, sensitivities and specificities may be somewhat lower in future routine scans, owing to the high heterogeneity of values observed in patients and controls. This, however, again corroborates the need for an observer-independent and objective approach as applied here, rather than simple visual analyses.

Furthermore, subjects with MCI and AD patients were slightly older than the healthy controls included in this study. Effects of age, however, did not appear of relevant contribution for the model generation in discriminant analyses, indicating that age effects are inferior to the effects of activity within the DMN and connectivity.

4.4. Conclusion

Our results have important implications on a potential future routine use of resting state fMRI in suspected AD. Time course correlation analyses seem to outperform independent component analyses in terms of diagnostic power in the identification of patients with Alzheimer's disease. However, multivariate analyses combining both methods of analysis by considering the activity of various parts of the DMN as well as the interconnectivity between these regions are required to achieve optimal and clinically acceptable diagnostic power. Interestingly, using this approach, the disease pattern observed in patients with AD can be identified in a high proportion of MCI subjects. There are some hints, that this test could be a noninvasive biomarker to identify the proportion of MCI subjects that will convert to AD, however, this needs to be validated in further follow-up studies with a higher number of subjects included.

Disclosure statement

The authors state that there are no actual or potential conflicts of interest.

Subjects' consent was obtained according to the Declaration of Helsinki. The study was approved by the ethics committee and the local authorities.

Acknowledgements

Funding was obtained through the Science Foundation Ireland (SFI) Stokes Programme (to AB), as well as through the SFI investigator neuroimaging programme grant 08/IN.1/B1846 (to HH).

References

Artero, S., Tierney, M.C., Touchon, J., Ritchie, K., 2003. Prediction of transition from cognitive impairment to senile dementia: a prospective, longitudinal study. Acta Psychiatr. Scand. 107, 390–393.

Beckmann, C.F., Smith, S.M., 2005. Tensorial extensions of independent component analysis for multisubject FMRI analysis. Neuroimage 25, 294–311.

Benjamini, Y., Hochberg, Y., 1995. Controlling the False Discovery Rate: A Practical and Powerful Approach to Multiple Testing. J. R. Stat. Soc. B 57, 289–300.

Binder, J.R., Frost, J.A., Hammeke, T.A., Bellgowan, P.S., Rao, S.M., Cox, R.W., 1999. Conceptual processing during the conscious resting state. A functional MRI study. J. Cogn. Neurosci. 11, 80–95.

Birn, R.M., Diamond, J.B., Smith, M.A., Bandettini, P.A., 2006. Separating respiratory-variation-related fluctuations from neuronal-activity-related fluctuations in fMRI. Neuroimage 31, 1536–1548.

Bluhm, R.L., Osuch, E.A., Lanius, R.A., Boksman, K., Neufeld, R.W., Theberge, J., Williamson, P., 2008. Default mode network connectivity: effects of age, sex, and analytic approach. Neuroreport 19, 887–891.

Braak, H., Braak, E., 1991. Neuropathological staging of Alzheimer-related changes. Acta Neuropathol. 82, 239–259.

Buckner, R.L., Snyder, A.Z., Shannon, B.J., laRossa, G., Sachs, R., Fotenos, A.F., Sheline, Y.I., Klunk, W.E., Mathis, C.A., Morris, J.C., Mintun, M.A., 2005. Molecular, structural, and functional characterization of Alzheimer's disease: evidence for a relationship between default activity, amyloid, and memory. J. Neurosci. 25, 7709–7717.

Buerger, K., Ewers, M., Andreasen, N., Zinkowski, R., Ishiguro, K., Vanmechelen, E., Teipel, S.J., Graz, C., Blennow, K., Hampel, H., 2005. Phosphorylated tau predicts rate of cognitive decline in MCI subjects: a comparative CSF study. Neurology 65, 1502–1503.

Conde, J.R., Streit, W.J., 2006. Microglia in the aging brain. J. Neuropathol. Exp. Neurol. 65, 199–203.

Damoiseaux, J.S., Beckmann, C.F., Arigita, E.J., Barkhof, F., Scheltens, P., Stam, C.J., Smith, S.M., Rombouts, S.A., 2008. Reduced resting-state brain activity in the "default network" in normal aging. Cereb. Cortex 18, 1856–1864.

Damoiseaux, J.S., Rombouts, S.A., Barkhof, F., Scheltens, P., Stam, C.J., Smith, S.M., Beckmann, C.F., 2006. Consistent resting-state networks across healthy subjects. Proc. Natl. Acad. Sci. U. S. A. 103, 13848–13853.

De Luca, M., Beckmann, C.F., De Stefano, N., Matthews, P.M., Smith, S.M., 2006. fMRI resting state networks define distinct modes of

long-distance interactions in the human brain. Neuroimage 29, 1359–1367.

De Santi, S., de Leon, M.J., Convit, A., Tarshish, C., Rusinek, H., Tsui, W.H., Sinaiko, E., Wang, G.J., Bartlet, E., Volkow, N., 1995. Age-related changes in brain: II. Positron emission tomography of frontal and temporal lobe glucose metabolism in normal subjects. Psychiatr. Q. 66, 357–370.

Delbeuck, X., Van der Linden, M., Collette, F., 2003. Alzheimer's disease as a disconnection syndrome? Neuropsychol. Rev. 13, 79–92.

Drzezga, A., Grimmer, T., Riemenschneider, M., Lautenschlager, N., Siebner, H., Alexopoulus, P., Minoshima, S., Schwaiger, M., Kurz, A., 2005. Prediction of individual clinical outcome in MCI by means of genetic assessment and (eighteen) F-FDG PET. J. Nucl. Med. 46, 1625–1632.

Drzezga, A., Lautenschlager, N., Siebner, H., Riemenschneider, M., Willoch, F., Minoshima, S., Schwaiger, M., Kurz, A., 2003. Cerebral metabolic changes accompanying conversion of mild cognitive impairment into Alzheimer's disease: a PET follow-up study. Eur. J. Nucl. Med. Mol. Imaging 30, 1104–1113.

Esposito, F., Bertolino, A., Scarabino, T., Latorre, V., Blasi, G., Popolizio, T., Tedeschi, G., Cirillo, S., Goebel, R., Di Salle, F., 2006. Independent component model of the default-mode brain function: Assessing the impact of active thinking. Brain Res. Bull. 70, 263–269.

Esposito, F., Scarabino, T., Hyvarinen, A., Himberg, J., Formisano, E., Comani, S., Tedeschi, G., Goebel, R., Seifritz, E., Di Salle, F., 2005. Independent component analysis of fMRI group studies by self-organizing clustering. Neuroimage 25, 193–205.

Fox, M.D., Snyder, A.Z., Vincent, J.L., Corbetta, M., Van Essen, D.C., Raichle, M.E., 2005. The human brain is intrinsically organized into dynamic, anticorrelated functional networks. Proc. Natl. Acad. Sci. U. S. A. 102, 9673–9678.

Fransson, P., 2005. Spontaneous low-frequency BOLD signal fluctuations: an fMRI investigation of the resting-state default mode of brain function hypothesis. Hum. Brain Mapp. 26, 15–29.

Fukunaga, M., Horovitz, S.G., van Gelderen, P., de Zwart, J.A., Jansma, J.M., Ikonomidou, V.N., Chu, R., Deckers, R.H., Leopold, D.A., Duyn, J.H., 2006. Large-amplitude, spatially correlated fluctuations in BOLD fMRI signals during extended rest and early sleep stages. Magn. Reson. Imaging 24, 979–992.

Garrity, A.G., Pearlson, G.D., McKiernan, K., Lloyd, D., Kiehl, K.A., Calhoun, V.D., 2007. Aberrant "default mode" functional connectivity in schizophrenia. Am. J. Psychiatry 164, 450–457.

Goebel, R., Esposito, F., Formisano, E., 2006. Analysis of functional image analysis contest (FIAC) data with brainvoyager QX: From single-subject to cortically aligned group general linear model analysis and self-organizing group independent component analysis. Hum. Brain Mapp. 27, 392–401.

Good, C.D., Johnsrude, I.S., Ashburner, J., Henson, R.N., Friston, K.J., Frackowiak, R.S., 2001. A voxel-based morphometric study of ageing in 465 normal adult human brains. Neuroimage 14, 21–36.

Grady, C.L., Furey, M.L., Pietrini, P., Horwitz, B., Rapoport, S.I., 2001. Altered brain functional connectivity and impaired short-term memory in Alzheimer's disease. Brain 124, 739–756.

Greicius, M.D., Flores, B.H., Menon, V., Glover, G.H., Solvason, H.B., Kenna, H., Reiss, A.L., Schatzberg, A.F., 2007. Resting-state functional connectivity in major depression: abnormally increased contributions from subgenual cingulate cortex and thalamus. Biol. Psychiatry 62, 429–437.

Greicius, M.D., Srivastava, G., Reiss, A.L., Menon, V., 2004. Default-mode network activity distinguishes Alzheimer's disease from healthy aging: evidence from functional MRI. Proc. Natl. Acad. Sci. U. S. A. 101, 4637–4642.

Hedges, L.V., Vevea, J.L., 1998. Fixed- and random-effects models in meta-analysis. Psychol. Methods 3, 486–504.

Horwitz, B., Grady, C.L., Schlageter, N.L., Duara, R., Rapoport, S.I., 1987. Intercorrelations of regional cerebral glucose metabolic rates in Alzheimer's disease. Brain Res. 407, 294–306.

Knopman, D.S., deKosky, S.T., Cummings, J.L., Chui, H., Corey-Bloom, J., Relkin, N., Small, G.W., Miller, B., Stevens, J.C., 2001. Practice parameter: diagnosis of dementia (an evidence-based review). Report of the Quality Standards Subcommittee of the American Academy of Neurology. Neurology 56, 1143–1153.

Koch, W., Teipel, S., Mueller, S., Buerger, K., Bokde, A.L., Hampel, H., Coates, U., Reiser, M., Meindl, T., 2010. Effects of aging on default mode network activity in resting state fMRI: Does the method of analysis matter? Neuroimage 51, 280–287.

McKeown, M.J., Makeig, S., Brown, G.G., Jung, T.P., Kindermann, S.S., Bell, A.J., Sejnowski, T.J., 1998. Analysis of fMRI data by blind separation into independent spatial components. Hum. Brain Mapp. 6, 160–188.

McKhann, G.M., Albert, M.S., Grossman, M., Miller, B., Dickson, D., Trojanowski, J.Q., 2001. Clinical and pathological diagnosis of frontotemporal dementia: report of the Work Group on Frontotemporal Dementia and Pick's Disease. Arch. Neurol. 58, 1803–1809.

Minoshima, S., Giordani, B., Berent, S., Frey, K.A., Foster, N.L., Kuhl, D.E., 1997. Metabolic reduction in the posterior cingulate cortex in very early Alzheimer's disease. Ann. Neurol. 42, 85–94.

Morris, J.C., Heyman, A., Mohs, R.C., Hughes, J.P., van Belle, G., Fillenbaum, G., Mellits, E.D., Clark, C., 1989. The Consortium to Establish a Registry for Alzheimer's Disease (CERAD). Part I. Clinical and neuropsychological assessment of Alzheimer's disease. Neurology 39, 1159–1165.

Mosconi, L., 2005. Brain glucose metabolism in the early and specific diagnosis of Alzheimer's disease. FDG-PET studies in MCI and AD. Eur. J. Nucl. Med. Mol. Imaging 32, 486–510.

Mosconi, L., Tsui, W.H., Herholz, K., Pupi, A., Drzezga, A., Lucignani, G., Reiman, E.M., Holthoff, V., Kalbe, E., Sorbi, S., Diehl-Schmid, J., Perneczky, R., Clerici, F., Caselli, R., Beuthien-Baumann, B., Kurz, A., Minoshima, S., de Leon, M.J., 2008. Multicenter standardized 18F-FDG PET diagnosis of mild cognitive impairment, Alzheimer's disease, and other dementias. J. Nucl. Med. 49, 390–398.

Mosconi, L., Tsui, W.H., Pupi, A., De Santi, S., Drzezga, A., Minoshima, S., de Leon, M.J., 2007. (eighteen) F-FDG PET database of longitudinally confirmed healthy elderly individuals improves detection of mild cognitive impairment and Alzheimer's disease. J. Nucl. Med. 48, 1129–1134.

Nordberg, A., 2004. Is amyloid plaque imaging the key to monitoring brain pathology of Alzheimer's disease in vivo? Eur. J. Nucl. Med. Mol. Imaging 31, 1540–1543.

Nordberg, A., 2008. Amyloid plaque imaging in vivo: current achievement and future prospects. Eur. J. Nucl. Med. Mol. Imaging 35 suppl 1, S46–S50.

Oldfield, R.C., 1971. The assessment and analysis of handedness: the Edinburgh inventory. Neuropsychologia 9, 97–113.

Petersen, R.C., 2004. Mild cognitive impairment as a diagnostic entity. J. Intern. Med. 256, 183–194.

Petersen, R.C., Doody, R., Kurz, A., Mohs, R.C., Morris, J.C., Rabins, P.V., Ritchie, K., Rossor, M., Thal, L., Winblad, B., 2001. Current concepts in mild cognitive impairment. Arch. Neurol. 58, 1985–1992.

Petersen, R.C., Smith, G.E., Ivnik, R.J., Tangalos, E.G., Schaid, D.J., Thibodeau, S.N., Kokmen, E., Waring, S.C., Kurland, L.T., 1995. Apolipoprotein E status as a predictor of the development of Alzheimer's disease in memory-impaired individuals. JAMA 273, 1274–1278.

Phelps, M.E., Schelbert, H.R., Mazziotta, J.C., 1983. Positron computed tomography for studies of myocardial and cerebral function. Ann. Intern. Med. 98, 339–359.

Raz, N., Gunning, F.M., Head, D., Dupuis, J.H., McQuain, J., Briggs, S.D., Loken, W.J., Thornton, A.E., Acker, J.D., 1997. Selective aging of the human cerebral cortex observed in vivo: differential vulnerability of the prefrontal gray matter. Cereb. Cortex 7, 268–282.

Rombouts, S.A., Damoiseaux, J.S., Goekoop, R., Barkhof, F., Scheltens, P., Smith, S.M., Beckmann, C.F., 2009. Model-free group analysis

shows altered BOLD FMRI networks in dementia. Hum. Brain Mapp. 30, 256–266.

Shulman, G.L., Corbetta, M., Buckner, R.L., Raichle, M.E., Fiez, J.A., Miezin, F.M., Petersen, S.E., 1997. Top-down modulation of early sensory cortex. Cereb. Cortex 7, 193–206.

Sorg, C., Riedl, V., Muhlau, M., Calhoun, V.D., Eichele, T., Laer, L., Drzezga, A., Forstl, H., Kurz, A., Zimmer, C., Wohlschlager, A.M., 2007. Selective changes of resting-state networks in individuals at risk for Alzheimer's disease. Proc. Natl. Acad. Sci. U. S. A. 104, 18760–18765.

Talairach, J.T.P., 1988. Co-Planar Stereotaxic Atlas of the Human Brain. Thieme, New York.

Tierney, M.C., Szalai, J.P., Snow, W.G., Fisher, R.H., Nores, A., Nadon, G., Dunn, E., St George-Hyslop, P.H., 1996a. Prediction of probable Alzheimer's disease in memory-impaired patients: A prospective longitudinal study. Neurology 46, 661–665.

Tierney, M.C., Szalai, J.P., Snow, W.G., Fisher, R.H., Tsuda, T., Chi, H., McLachlan, D.R., St George-Hyslop, P.H., 1996b. A prospective study of the clinical utility of ApoE genotype in the prediction of outcome in patients with memory impairment. Neurology 46, 149–154.

Wang, K., Liang, M., Wang, L., Tian, L., Zhang, X., Li, K., Jiang, T., 2007. Altered functional connectivity in early Alzheimer's disease: a resting-state fMRI study. Hum. Brain Mapp. 28, 967–978.

Wang, L., Zang, Y., He, Y., Liang, M., Zhang, X., Tian, L., Wu, T., Jiang, T., Li, K., 2006. Changes in hippocampal connectivity in the early stages of Alzheimer's disease: evidence from resting state fMRI. Neuroimage 31, 496–504.

Whitwell, J.L., Jack, C.R., Jr, 2005. Comparisons between Alzheimer disease, frontotemporal lobar degeneration, and normal aging with brain mapping. Top. Magn. Reson. Imaging 16, 409–425.

Willis, M.W., Ketter, T.A., Kimbrell, T.A., George, M.S., Herscovitch, P., Danielson, A.L., Benson, B.E., Post, R.M., 2002. Age, sex and laterality effects on cerebral glucose metabolism in healthy adults. Psychiatry Res. 114, 23–37.